Chapter 14. Marine Atmospheric Boundary Layer Cellular Convection and Longitudinal Roll Vortices

Todd D. Sikora
United States Naval Academy, Department of Oceanography, Annapolis, MD, USA

Susanne Ufermann
Laboratory for Satellite Oceanography, Southampton Oceanography Centre, Southampton, United Kingdom

14.1 Introduction

The marine atmospheric boundary layer (MABL) is that part of the atmosphere that has direct contact and, hence, is directly influenced by the ocean. Thus, the MABL is where the ocean and atmosphere exchange large amounts of heat, moisture, and momentum, primarily via turbulent transport [*Fairall et al.*, 1996]. Couplets of cellular updrafts and downdrafts (cells) and couplets of roll-like updrafts and downdrafts (rolls) in the atmospheric boundary layer represent the organization of these turbulent fluxes. Thus, cells and rolls over the ocean are coherent structures of enhanced air-sea interaction [*Khalsa and Greenhut*, 1985]. These coherent structures can be initiated thermodynamically (i.e. buoyancy-driven) and / or dynamically (i.e. wind shear-driven).

Cells and rolls each have distinctive signatures on the ocean surface. These signatures are the result of the alteration of the ocean surface roughness on the cm-scale that result from gusts of wind emanating from the downdrafts of the coherent structures. These gusts result from the mixing of high-momentum air from aloft downwards towards the sea surface. At the same time, the updrafts tend to transport low-momentum air upwards. Thus both of these processes cause a negative turbulent momentum flux. In contrast to this, heat and moisture fluxes can be either positive or negative since the updrafts and downdrafts that induce momentum mixing can be hot or cold and moist or dry relative to the mean environment.

As has been described in earlier chapters, synthetic aperture radar (SAR) senses the cm-scale (Bragg) wave spectrum and, hence, cm-scale sea surface roughness at a resolution on order 10 m to 100 m over a swath width on order 100 km to 1000 km. Changes in wind speed and direction change the Bragg wave energy spectrum via the turbulent momentum flux between the atmosphere and ocean surface. Radar backscatter increases with wind speed. The highest signal return is obtained when looking in an upwind direction. At the same time, the intervening atmosphere is mainly transparent to SAR, although precipitation can at times affect the radar signal (reviewed by *Alpers and Melsheimer* (Chapter 17) and in *Melsheimer et al.* [1998, 2001]). Thus, spaceborne SAR is capable of providing a detailed view of sea surface roughness patterns of various meteorological phenomena, including cells and rolls.

This chapter will describe the phenomena of MABL cells and rolls from a SAR perspective. It will examine their causes and structure, their signatures in SAR imagery, and what information can be extracted from those signatures. Knowledge of the spatial and temporal distribution, as well as intensity, of cells and rolls is particularly important to meteorologists and oceanographers. On the microscale (< 2 km) and mesoscale (2 km to 2000 km), cells and rolls can lead to organized convective precipitation. In mesoscale and macroscale (2000 km to 20,000

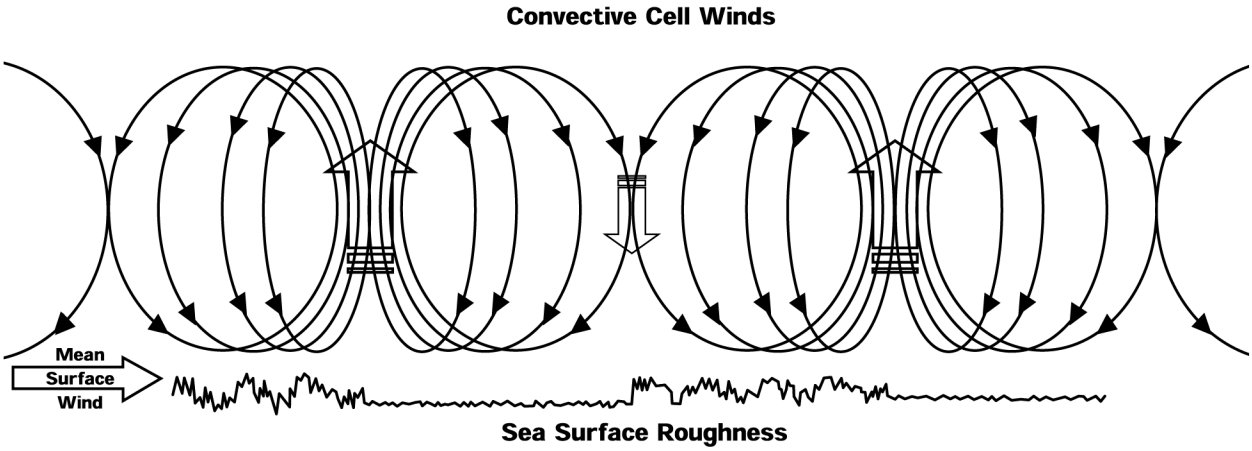

Figure 14.1. Vertical cross section through an atmospheric convective cells above the ocean surface. The figure shows the cell-induced (perturbation) flow pattern and the resulting sea surface roughness after interaction with the mean surface wind. In this case where the magnitude of the mean surface wind approximately equals that of the cell-induced wind beneath the convective cell. Sea surface roughness (and resulting radar backscatter) are increased where the cell winds and mean surface wind are in the same direction minimized when they are opposed.

km) weather forecasting models, the spatial distribution of turbulent fluxes (and, hence, cells and rolls) appears as required terms in the governing equations. On very long temporal scales, the statistical representation of cells and rolls becomes important in climate modeling.

14.2 Cells

Cells in the MABL can form under relatively light wind conditions over those regions of the ocean that have a negative air-sea temperature difference (i.e. where the sea surface temperature is higher than the air temperature directly above the ocean). As a result of this unstable stratification, convective up- and downdrafts develop. At the sea surface, this either causes cell-induced low-momentum air flow directed radially inwards (towards an updraft) or high-momentum air flow directed radially outwards (away from a downdraft) over a circular area with a diameter on the order of a few to up to several tens of kilometers.

As illustrated in Figure 14.1, the wind field of a cell is usually superimposed on a more homogenous ambient wind field. A cell's radial wind vectors are thus in line with the ambient wind on one side of the cell, and they oppose the ambient wind on the opposite side of the cell. Thus, the resulting total wind speed just above the ocean is higher on one side of the cell than on the other, resulting in an increased and decreased intensity of Bragg waves. Therefore, atmospheric cells over the ocean usually produce a mottled signature in SAR images that is brighter than the background signal on one side of the cell, and darker than the background signal on the other side of the cell [*Mitnik*, 1992; *Sikora et al.*, 1995; *Zecchetto et al.*, 1998].
The exact shape of an individual mottle element and its resulting SAR signature are not only affected by local wind speed and wind direction, but also by the SAR frequency, SAR incident angle, and the SAR look direction [*Mitnik*, 1992; *Ufermann and Romeiser*, 1999b]. Moreover, recent research has shown that differences in the SAR imaging mechanism at vertical and horizontal polarization can affect the imaging of both atmospheric and oceanic phenomena. Wind variations on short spatial scales, such as the ones generated by convection cells (and rolls), mainly modulate the short surface (Bragg) waves, whereas hydrodynamic modulation by

Figure 14.2. A SAR image (scaled for presentation) acquired from RADARSAT-1 (C-band, HH) on 17 January 1997 at 2242 UTC off the east coast of the United States when the MABL stratification was unstable. The image contains the mottled SAR-signature of convection throughout. The imaged area is 300 km x 300 km centered at approximately at 35.7°N, 72.0°W. The top of the image is directed towards 348°. ©CSA 1997

oceanic phenomena predominantly acts on longer (decimeter to meter) waves. As shown by *Romeiser and Alpers* [1997], contributions of the Bragg waves to the backscatter are similar at vertical and horizontal polarization, whereas the relative contribution of the long waves to the backscatter is larger at horizontal than at vertical polarization. As a result, oceanic phenomena produce stronger SAR signatures at horizontal than at vertical polarization. This polarization-dependence can be exploited to separate contributions of oceanic and atmospheric phenomena to the radar signal [*Ufermann and Romeiser*, 1999a]. Moreover, recent research has shown that differences in the SAR imaging mechanism at vertical and horizontal polarization can affect the imaging of both atmospheric and oceanic phenomena. Wind variations on short spatial scales,

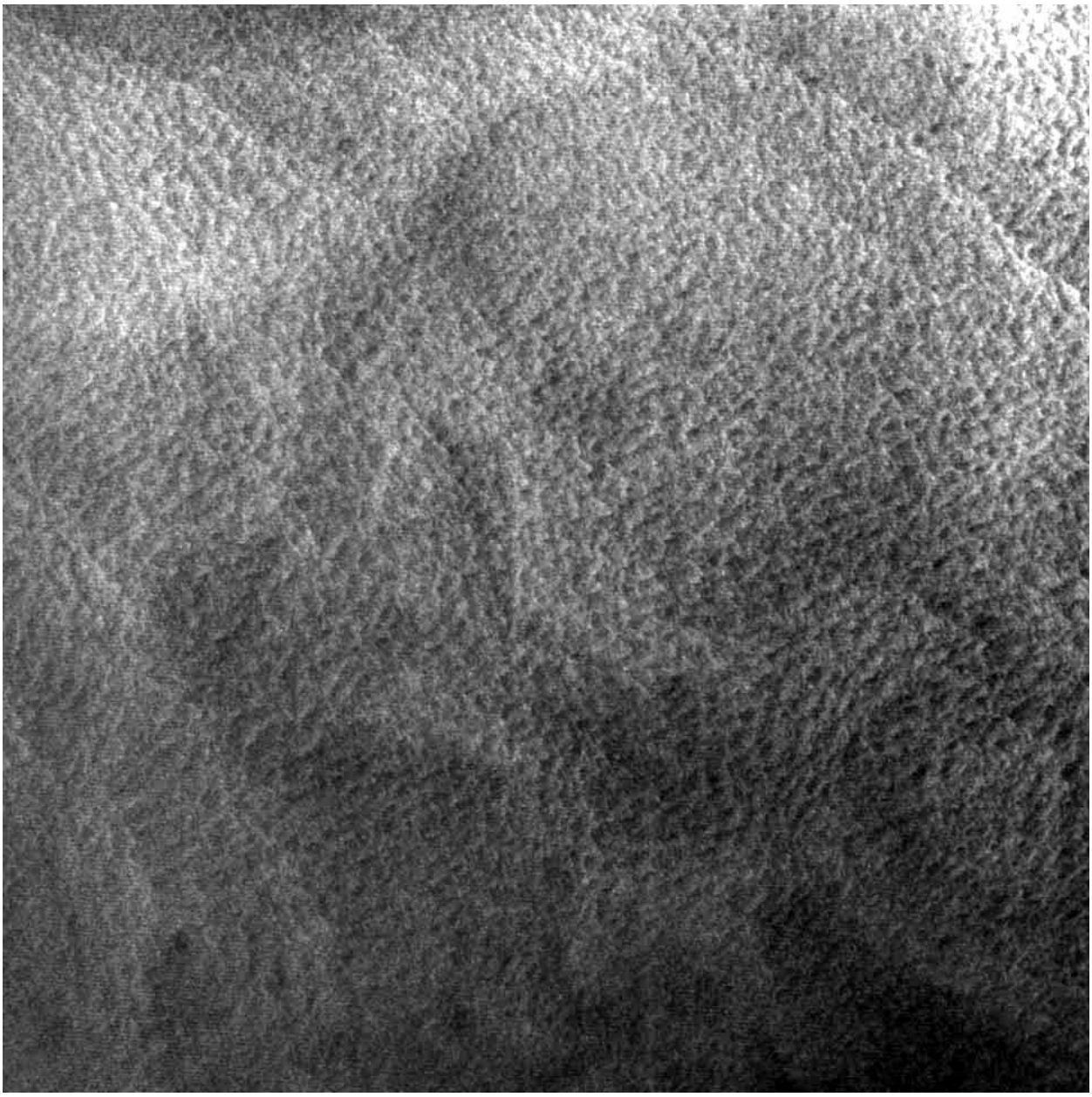

Figure 14.3. An example of a mottled SAR image (scaled for presentation) acquired from RADARSAT-1 (C-band, HH) 06 March 1997 at 2242 UTC off the east coast of the United States when the MABL stratification was unstable. The imaged area is 300 km x 300 km centered at approximately at 37.3°N, 72.8°W. The top of the image is directed towards 348°. ©CSA 1997

such as the ones generated by convection cells (and rolls), mainly modulate the short surface (Bragg) waves, whereas hydrodynamic modulation by oceanic phenomena predominantly acts on longer (decimeter to meter) waves.

A field of mottling on SAR imagery tends to be quite similar in appearance to what a field of cumulus clouds looks like on visible satellite imagery because the cumulus clouds and clear spaces between them represent the tops of the updraft / downdraft couplets that produce the surface SAR scene. We point out, however that clouds need not be present in order for SAR to sense the presence of cells.

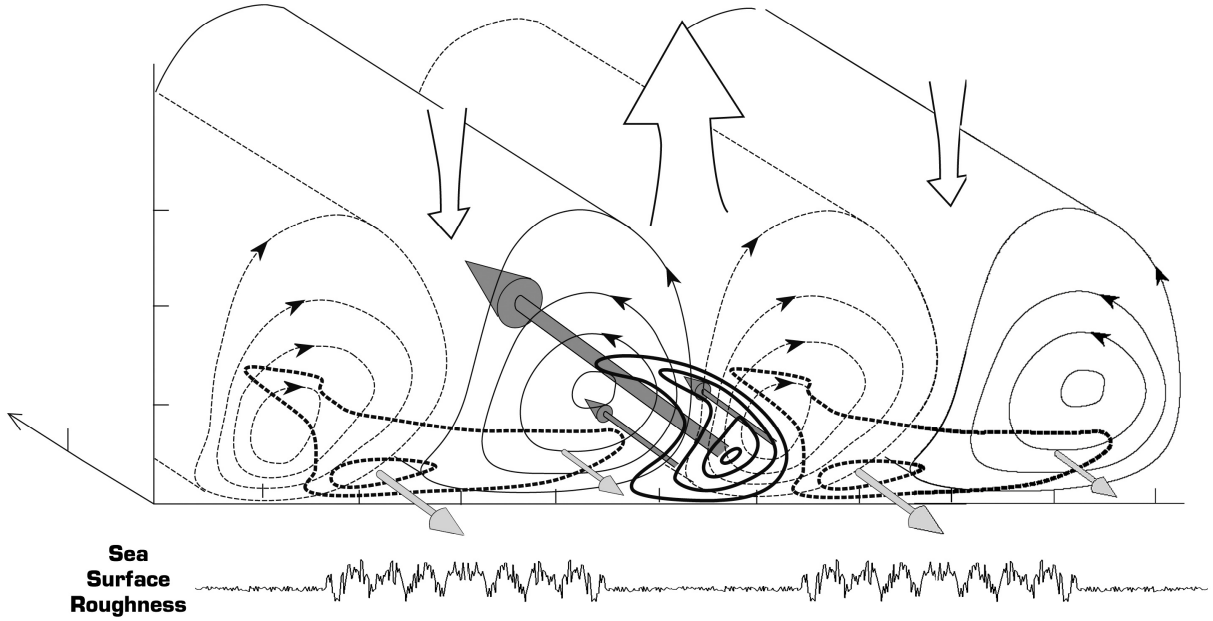

Figure 14.4. Three-dimensional view of idealized roll vortices above the sea surface and the corresponding roll-induced (perturbation) flow pattern. Height increases towards the top of the page. The light dashed arrows are roll-induced stream lines in the vertical-cross roll plane. The tubular arrows are roll-induced wind vectors along the axis of the rolls. The heavy dashed lines are roll-induced isotachs along the axis of the rolls. Finally, the roll-induced vertical velocity pattern is represented by the open arrows above the rolls. The mean wind shear vector is along the axis of the rolls and out of the page. The sea surface roughness variations are shown along the bottom. Roughness (and SAR backscatter) are highest under the descending regions. Provided courtesy of Dr. Ralph Foster, University of Washington Applied Physics Laboratory.

Figure 14.2 shows an example of a SAR image (scaled for presentation) acquired from RADARSAT-1 at C-band, horizontal polarization on 17 January 1997 at 2242 UTC off the east coast of the United States when the MABL stratification was unstable according to buoy data near the imaged area. The image contains the mottled SAR signature of convection throughout. The image is 300 km by 300 km and is centered approximately at 35.7°N, 72.0°W. The top of the image is directed towards 348°.

Another example of a mottled SAR scene can be seen in Figure 14.3, which was acquired from RADARSAT-1 at C-band, horizontal polarization on 06 March 1997 at 2242 UTC off the east coast of the United States. The image is 300 km by 300 km and is centered approximately at 37.3°N, 72.8°W. The top of the image is directed towards 348°. Buoy data in the imaged area indicate an unstable stratification of the MABL at the time of image acquisition.

14.3 Rolls

As their name implies, longitudinal rolls vortices are quasi-helical circulations. *Etling and Brown* [1993] and *Young et al.* [2002] provide thorough reviews of rolls. The most commonly cited mechanism for roll development is thermodynamic instability in an environment with sufficient wind shear (what is sufficient is addressed below) and it is this type of roll that we discuss here. We point out, however, that other roll-initiation mechanisms exist. We refer the reader to *Etling and Brown* [1993] and *Young et al.* [2002] for further reading on this subject.

Figure 14.4 is a schematic of an idealized field of roll vortices. The axes of the boundary layer rolls are oriented parallel to the mean boundary layer wind shear vector. Ascending and

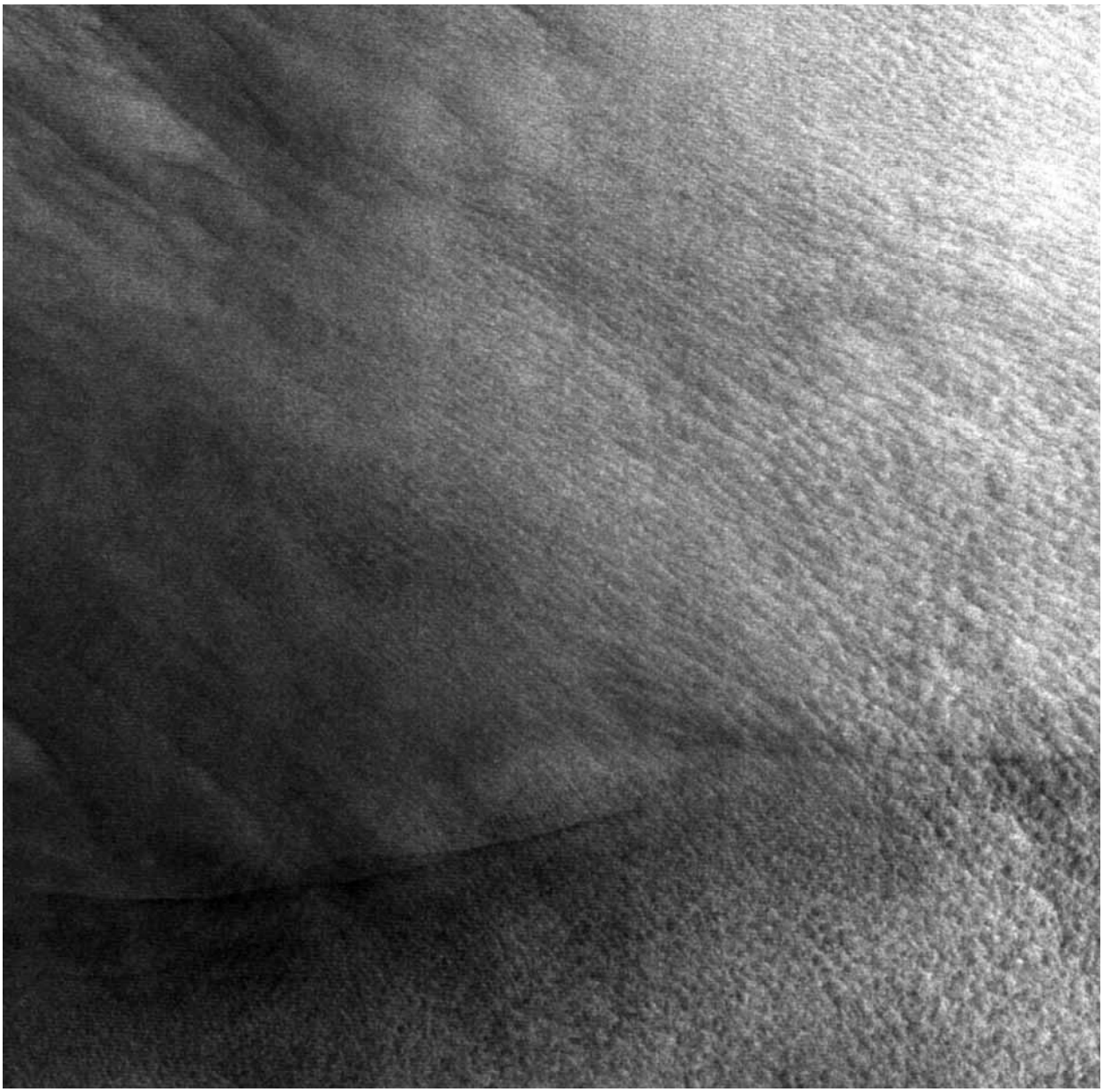

Figure 14.5. SAR image (scaled for presentation) acquired from RADARSAT-1 (C-band, HH) on 06 March 1997 at 2242 UTC off the east coast of the United States when the MABL stratification was unstable and moderate winds were present. The image contains the SAR-signature of roll vortices throughout its upper right-hand portion. The imaged area is 300 km x 300 km and centered at approximately at 35.7°N, 72.0°W. The top of the image is directed towards 348°. ©CSA 1997

descending regions of the circulation lead to corresponding decreased and increased sea surface roughness in the same manner as was described for cellular convection, resulting in lines of enhanced and decreased backscatter with the lines of enhanced backscatter effectively being the linear organization of mottle elements [e.g., *Alpers and Brümmer*, 1994; *Mourad*, 1996; *Mourad and Walter*, 1996; *Müller et al.*, 1999; *Babin et al.*, 2003]. This is quite similar to what a field of roll-induced clouds looks like on a visible satellite image. This is expected because the lines of

clouds and clear regions between them represent the locations of the ascending and descending branches of the rolls that produce the surface SAR scene. Along any particular cloud line, there is variability in the degree of convection and, hence, the texture of the cloud field. We point out, however that clouds need not be present in order for SAR to sense the presence of rolls.

Figure 14.5 shows a SAR image (scaled for presentation) acquired from RADARSAT-1 at C-band, horizontal polarization on 06 March 1997 at 2242 UTC off the east coast of the United States when the MABL stratification was unstable and moderate winds were present. The image is 300 km by 300 km and is centered approximately at 35.7°N, 72.0°W. The top of the image is directed towards 348°. The image contains the SAR-signature of roll vortices throughout its upper-right portion. The scale of the rolls in the direction perpendicular to their long axis is on the order of 1 to 10 km.

14.4 Transition Between Cells and Rolls

As the ratio of buoyancy to shear (approximated by the ratio of air-sea temperature difference to mean wind speed) increases beyond some threshold value, rolls develop into cellular convection [e.g., *Weckwerth et al*., 1999]. The precise threshold value for this transition is still a topic for debate [*Young et al*., 2002]. However, SAR imagery may be employed to study this transition in unprecedented spatial detail and without the need for the existence of clouds that many previous studies have relied on.

An example of a SAR image showing the transition from rolls to cells can be found in Figure 14.6. Figure 14.6a is a RADARSAT-1 SAR image (scaled for presentation) acquired at C-band, horizontal polarization. The image was acquired at 2229 UTC on 14 January 1997 during a cold-air outbreak off the northeast coast of the United States. It covers an area of 900 km by 300 km and is centered approximately at 38.2°N, 69.9°W. The top of the image is directed towards 348^{o}. Nearby NOAA buoys reported air-sea temperature differences changing from –9.4°C to –12.4°C from the top to the bottom of the image while the winds remained relatively constant across the swath, blowing out of the northwest at 7 to 8 ms^{-1}. Hence, there is evidence that the ratio of buoyancy to shear increases from the top to the bottom of the image.

Near the top left hand side of the image, 1 km scale mottles appear to be aligned in rows extending from the upper left towards the lower right, similar to what was seen in the imagery of Figure 14.5. As distance increases towards the lower right, the size of the individual mottled elements within a particular roll signature increases. *Babin et al.* [2003] attribute increase in scale to the corresponding decrease in static stability, as evidenced by decreased air-sea temperature differences reported by the buoys, or due to increased latent heating.

About one half of the way down from the top of the image, a dramatic change in the backscatter signature of the roll / mottled pattern begins. There, the mottle elements start to evolve into mesoscale (order 10 km) blister-like features. This transition occurs once the air flowing towards the southeast has crossed the Gulf Stream North Wall (the dark bowed line seen cutting across the middle of the scene). The corresponding Advanced Very High Resolution Radiometer (AVHRR) image (Figure 14.6b, Channel 1, 2 and 4 composite from 2327 UTC) shows the cloud-signature of the above-mentioned transition. In the lower right hand corner of the SAR image, these mesoscale blisters have completely replaced the roll signatures. *Babin et al.* [2003] argue that the blister-like pattern is the SAR-signature of mesoscale cellular convection. We refer the reader to *Atlas and Black* [1994], *Mourad and Walter* [1996], and *Katsaros et al.* [2000]. These articles contain additional discussions on SAR's ability to sense mesoscale cellular convection.

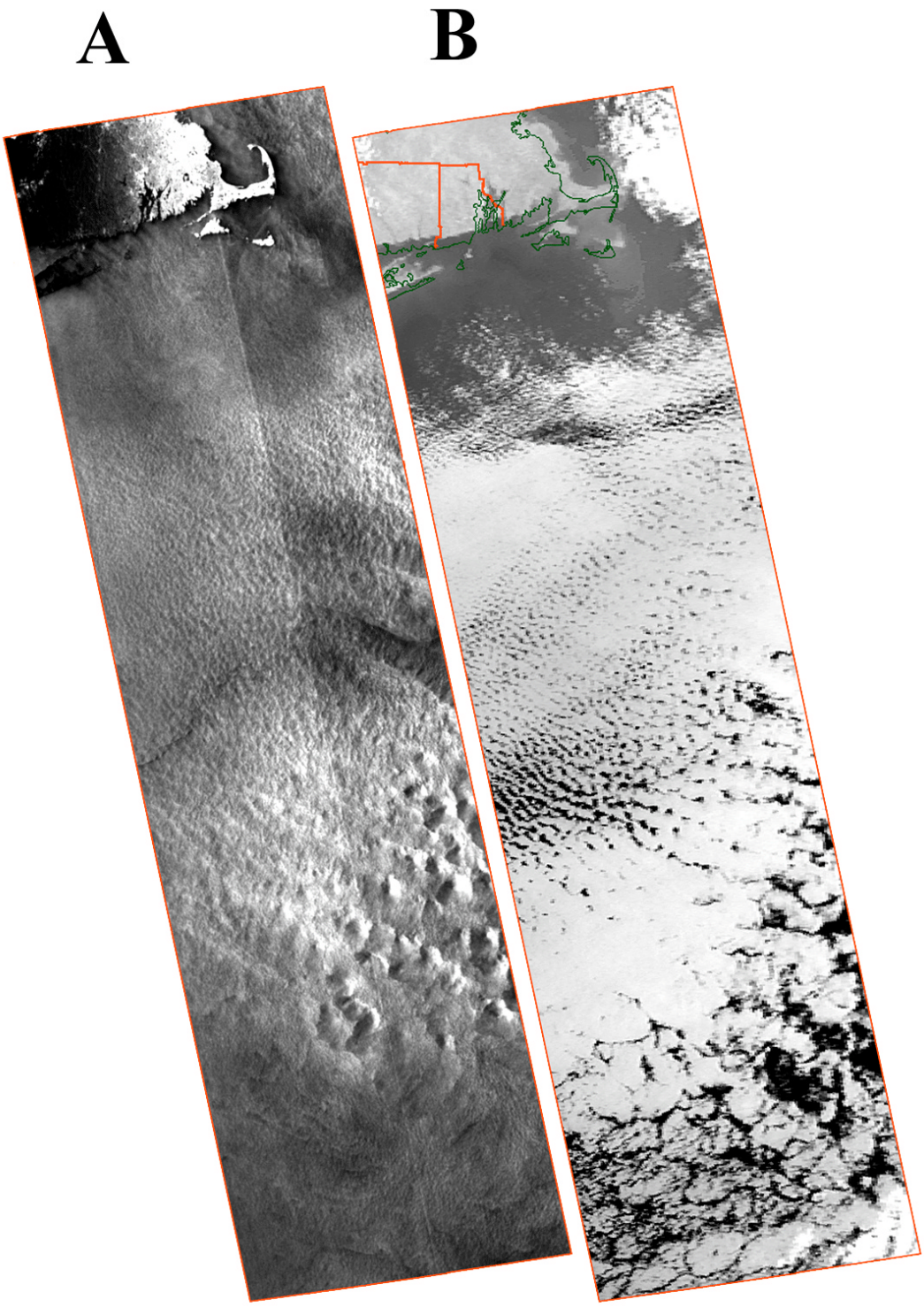

Figure 14.6. A) An example of a SAR image (scaled for presentation) acquired from RADARSAT-1 (C-band, HH) on 14 January 1997 at 2229 UTC during a cold air outbreak off the east coast of the United States. The area covered by each image is 300 km x 900 km and centered at approximately at 38.2°N, 69.9°W. The top of the image is directed towards 348°. ©CSA 1997; B) Corresponding AVHRR image (Channel 1, 2 and 4 composite), acquired at 2327 UTC on 14 January 1997. [After *Babin et al*., 2003]

14.5 Turbulent Flux Measurements from SAR Imagery

Here, we leave the reader with some thoughts on the potential of using SAR-derived wind speed imagery of MABL convection to derive turbulent fluxes of momentum and buoyancy. The SAR-derived wind imagery discussed in this book (e.g. *Monaldo and Beal* (Chapter 13)) is, strictly speaking, 10 m statically neutral wind imagery. In the presence of non-neutral conditions, there is a need to correct the neutral SAR-derived wind for the influence of static stability. This correction could be as much as 10 % for moderate wind speeds and negative air-sea temperature differences [*Young et al*., 2000]. *Young et al*. [2000] present a stability correction technique for statically unstable conditions that is based on the boundary layer depth, the friction velocity, and the standard deviation of the along-mean flow wind component, which is a function of the degree of mottling caused by a field of cells or rolls. A by-product of this stability correction technique is the Obukhov length which, when combined with sea surface temperature data, can be used to calculate a buoyancy flux. *Young et al.* [2000] and *Sikora and Thomson* [2002] show promising results from this technique and further testing is ongoing. The implication is that it might be possible to employ SAR imagery to generate high-resolution turbulent flux data over marine environments where the in-situ data is sparse. Such data can then be used to aid meteorologists and oceanographers in the research areas outlined in the Introduction.

14.6 References

Alpers, W., and B. Brümmer, 1994: Atmospheric boundary layer rolls observed by the synthetic aperture radar aboard the ERS-1 satellite. *J. Geophys. Res.,* **99,** 12 613–12 621.

Atlas, D., and P. G. Black, 1994: The evolution of convective storms from their footprints on the sea as viewed by synthetic aperture radar from space. *Bull. Amer. Meteor. Soc.*, **75**, 1183–1190.

Babin, S. M., T. D. Sikora, and N. S. Winstead, 2003: A case study of satellite synthetic aperture radar signatures of spatially evolving atmospheric convection over the western Atlantic Ocean. *Boundary-Layer Meteor.,* **106**, 527-546.

Etling, D., and R. A. Brown, 1993: Roll vortices in the planetary boundary layer: A review. *Boundary-Layer Meteor.*, **65**, 215–248.

Fairall, C. W., E. F. Bradley, D. P. Rogers, J. B. Edson, and G. S. Young, 1996: Bulk parameterization of air–sea fluxes for Tropical Ocean-Global Atmosphere Coupled-Ocean Atmosphere Response Experiment. *J. Geophys. Res*., **101**, 3747–3764.

Katsaros, K. B., P. W. Vachon, P. G. Black, P. P. Dodge, and E. W. Uhlhorn, 2000: Wind fields from SAR: could they improve our understanding of storm dynamics? *Johns Hopkins APL Tech. Dig.*, **21**, 86–93.

Khalsa, S. J. S., and G. K. Greenhut, 1985: Conditional sampling of updrafts and downdrafts in the marine atmospheric boundary layer. *J. Atmos. Sci.*, **42**, 2550–2562.

Melsheimer, C., W. Alpers, and M. Gade, 1998: Investigation of multifrequency/multipolarization radar signatures of rain cells over the ocean using SIR-C/X-SAR data. *J. Geophys. Res.*, **103**, 18 867–18 884.

——, ——, and ——, 2001: Simultaneous observations of rain cells over the ocean by the synthetic aperture radar aboard the ERS satellites and by surface-based weather radars. *J. Geophys. Res.*, **106**, 4665–4677.

Mitnik, L.M., 1992: Mesoscale coherent structures in the surface wind field during cold air outbreaks over the far eastern seas from the satellite side looking radar. *La Mer*, **30**, 287–296.

Mourad, P. D, 1996: Inferring multiscale structure in atmospheric turbulence using satellite-based synthetic aperture radar. *J. Geophys. Res.*, **101**, 18 433–18 449.

——, and B. A. Walter, 1996: Viewing a cold air outbreak using satellite-based synthetic aperture radar and advanced very high resolution radiometer imagery. *J. Geophys. Res.*, **101**, 16 391–16 400.

Müller, G., B. Brümmer, and W. Alpers, 1999: Roll convection within an Arctic cold-air outbreak: interpretation of in situ aircraft measurements and spaceborne SAR imagery by a three-dimensional atmospheric model. *Mon. Wea. Rev*., **127**, 363–380.

Romeiser, R., and W. Alpers, 1997: An improved composite surface model for the radar backscattering cross section of the ocean surface Part 2: Model response to surface roughness variations and the radar imaging of underwater bottom topography. *J. Geophys. Res.*, **102**, 25 251-25 267.

——, S. Ufermann, A. Androssov, H. Wehde, L. Mitnik, S. Kern, and A. Rubino, 2003: Interpretation of convection cell signatures in radar images of the Greenland Sea. *J. Geophys. Res.*, in press.

Sikora, T. D., and D. R. Thompson, 2002: Air–sea turbulence statistics from synthetic aperture radar: An update. *Can. J. Remote Sens.*, **28**, 517-523.

——, G. S. Young, R. C. Beal, and J. B. Edson, 1995: Use of spaceborne synthetic aperture radar imagery of the sea surface in detecting the presence and structure of the convective marine atmospheric boundary layer. *Mon. Wea. Rev.*, **123**, 3623–3632.

Ufermann, S., and R. Romeiser, 1999a: A new interpretation of multifrequency / multipolarization radar signatures of the Gulf Stream front. *J. Geophys. Res.*, **104**, 25 697-25 705.

——, and ——, 1999b: Numerical study on signatures of atmospheric convective cells in radar images of the ocean. *J. Geophys. Res*., **104**, 25 707–25 719.

Weckwerth, T. M., T. W. Horst, and J. W. Wilson, 1999: An observational study of the evolution of horizontal convective rolls. *Mon. Wea. Rev.*, **127**, 2160–2179.

Young, G. S., T. D. Sikora, and N. S. Winstead, 2000: Inferring marine atmospheric boundary layer properties from spectral characteristics of satellite-borne SAR imagery. *Mon. Wea. Rev.*, **128**, 1506–1520.

——, G. S., D. A. R. Kristovich, M. R. Hjelmfelt, and R. C. Foster, 2002: Rolls, streets, waves, and more: A review of quasi-two dimensional structures in the atmospheric boundary layer. *Bull. Amer. Meteor. Soc.*, **83**, 997–1001.

Zecchetto, S., P. Trivero, B. Fiscella, and P. Pavese, 1998: Wind stress structure in the unstable marine surface layer detected by SAR. *Boundary-Layer Meteor*., **86,** 1–28.